Impact of Precursor Compounds Associated with Long-Range Transport in the East Asia Region—Variation in CO/CO$_2$ and VOCs

Minwook Kim [1,†], **Myoungki Song** [2,†], **Sea-Ho Oh** [2], **Geun-Hye Yu** [2], **Seoyeong Choe** [2], **Hajeong Jeon** [2], **Jin-Ho Kim** [1] **and Min-Suk Bae** [2,*]

[1] Climate Change Assessment Division, National Institute of Agricultural Sciences, Wanju 55365, Republic of Korea; minuk09@korea.kr (M.K.); water86@korea.kr (J.-H.K.)

[2] Department of Environmental Engineering, Mokpo National University, Muan 58554, Republic of Korea; msong@mnu.ac.kr (M.S.); fanygh89@mnu.ac.kr (S.-H.O.); osh9119mnudk@mnu.ac.kr (G.-H.Y.); S184221@365.mokpo.ac.kr (S.C.); S214210@365.mokpo.ac.kr (H.J.)

[*] Correspondence: minsbae@mnu.ac.kr; Tel.: +82-61-450-2485

[†] These authors contributed equally to this work.

Abstract: In this study, the impact of long-range transport, one of the factors contributing to the presence of PM$_{2.5}$, was examined, and an analysis of marker compounds associated with its long-range transport was conducted. Aerosol optical depth, wind field, CO/CO$_2$ back-trajectory analysis, and satellite observation results were performed to determine PM$_{2.5}$, volatile organic compound (VOC), CO, CO$_2$, SO$_2$, O$_3$, NO, NO$_2$, and NH$_3$ levels at an orchard located in Jeollabuk-do, Republic of Korea. The characteristic of long-range transport at the observation area was evaluated during the research period. The concentrations for long-range transport based on concentration changes in gaseous materials and composition changes in PM$_{2.5}$ were analyzed. A back-trajectory analysis for the ratio of CO to CO$_2$ with satellite observation results was used to identify long-range transport. Furthermore, the proportionality between the ratio of 1,2-dichloroethane to naphthalene in VOCs and the quantity of precursor compounds linked to long-range transport were observed.

Keywords: VOC; long range transport; aged PM; 1,2-dichloroethane

1. Introduction

Air pollution aggravated by urban development and modernization is of a significant public health concern due to its adverse effects on human health. According to recent studies, an increase in PM$_{10}$ by about 10 μ/m^3 in concentration causes an increase of 0.58% in respiratory mortality, and an increase in PM$_{2.5}$ by 10 μ/m^3 increases the incidence and hospitalization of respiratory diseases by 2.07% and 8%, respectively [1,2]. In addition, a previous study indicated that 9.98% of the total deaths in China in 2016 were associated with exposure to PM$_{2.5}$ as well as an economic loss of 0.91% of the GDP (gross domestic product) [3]. Thus, nations around the world are making various efforts to reduce air pollutants.

Air pollutants are classified by gaseous and particulate matter. Chemical compounds of particulate matter include organic compounds, elemental carbon (EC), trace elements, and water-soluble ionic compounds [4–6]. Gaseous compounds such as VOCs (volatile organic compounds) including benzene and toluene are also mixed in the air, thus affecting air quality. These air pollutants can move in long-range transport depending on wind direction or speed, causing serious environmental issues and aging symptoms according to their retention time [7,8]. Thus, it is necessary to understand not only the features of regional air pollutants but also the external effects of long-range transport.

Various prior studies related to the long-range transport of atmospheric pollutants have been conducted. It has been argued that desert dust significantly contributes to the

increase in PM concentrations across Europe and that long-range transport contributes to approximately 50% of urban atmospheric pollutants [9–11]. Furthermore, according to previous research, South Korea, the study area of this investigation, has been documented as a recipient of various atmospheric pollutants, including PM and secondary fine particulate matter, as well as gaseous substances such as CO, originating from China [12–14]. Therefore, in order to comprehend the sources of atmospheric pollutants for mitigation purposes, it is essential to understand the long-range transport of key pollutants, their potential origins, and the relationship between pollutants and meteorological parameters. Various studies related to the long-range transport of air pollutants have insisted that desert dust contributes to increases in PM concentrations all over Europe and that approximately 50% of air pollutants in cities are due to long-range transport [7,9–11]. Various air pollutants such as PM, secondary pollutants, and gaseous matters such as CO from East Asia can flow into Korea, the research area of this study [12–18]. It is necessary to understand the relationship of long-range transport with potential sources and weather parameters of pollutants to reduce air pollutants. Thus, the purpose of this study was to analyze precursor compounds of air pollutants associated with long-range transport. An agricultural location without major point sources was selected to measure air pollutants increased by long-range transport. The results of this study might explain the long-range transport of air pollutants.

2. Materials and Methods

2.1. Measuring Location

An observational study was executed in an apple orchard located at Jangsoo, Jeollabuk-do, Korea ($35°62'04''$ N $127°51'24''$ E), to determine sources and features of $PM_{2.5}$ in an agricultural area. Observations were conducted for a total of 14 days from 25 January 2021 to 7 February 2021, during the winter period when long-distance inflows mainly occur [12–14]. A trailer for air measurement was used for observation (Figure 1). This trailer could collect custom-made, three-hour integrated PM using filters, VOCs using thermal desorption tubes (a total of 112 samples for each PM and VOCs), and gaseous compounds (CO, CO_2, SO_2, O_3, NO, NO_2 (Thermo Scientific, Waltham, MA, USA) and NH_3 (Los Gatos Research (LGR), ABB Inc., San Jose, CA, USA) using a real-time analyzer.
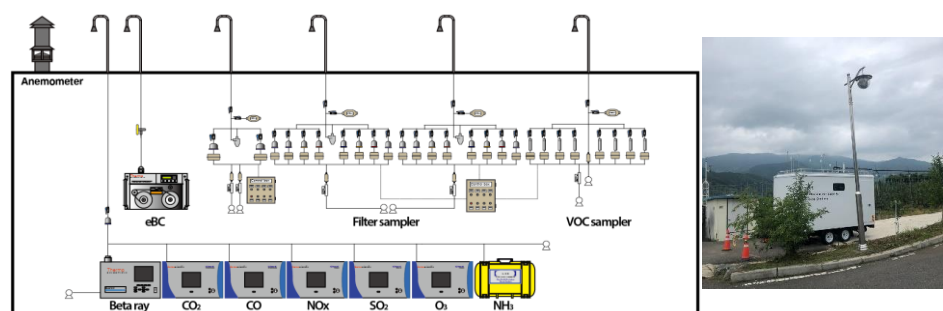
Figure 1. A trailer for air measurement located at Jangsoo in Jeollabuk-do, Korea (**Left**: Internal structure, **right**: installation view).

2.2. Chemical Analysis of $PM_{2.5}$

$PM_{2.5}$ was automatically collected every three hours during this study. The following compounds were analyzed to investigate the chemical compositions of $PM_{2.5}$: organic carbon (OC), EC, equivalent black carbon (eBC), water-soluble organic carbon (WSOC), water-soluble ionic compounds including NO_3^-, SO_4^{2-}, NH_4^+, and trace elements (i.e., Al, Si, Ca, and Ti). The NIOSH 5040 protocol (National Institute of Occupational Safety and Health, Washington, DC, USA) was used for the analysis of OC and EC. A multi-angle absorption photometer (MAAP) (Thermo Scientific 5012) was used for eBC analysis. After extracting collected filters with deionized distilled water (DDW), analyses of WSOC and water-soluble ionic compounds were performed with a total organic carbon (TOC) analyzer and ion chromatography (IC) (Metrohm 930, Herisau, Switzerland). Energy dispersive

X-ray fluorescence (ED–XRF, ARL QUANT'X EDXRF Spectrometer, Thermo Inc., Waltham, MA, USA) was used to analyze trace elements.

2.3. Analysis of VOCs

A three-hour integrated sequence VOC sampler was implemented at a flow rate of 50 mL/min to minimize the loss of low VOCs, which were automatically collected. A total of 123 samples were collected and analyzed during the sampling periods. VOCs (Custom (Q-QC27-1), Kemidas (M-VAVOC 503M2), Gyeonggi-do, Republic of Korea) were used as standard material for analysis. The internal standard material was chlorobenzene-d5 manufactured by Kemidas. A solid adsorption tube (C2-CAXX-5149) (Markes International, Ltd., Bridgend, UK) was utilized for sample collection and the calibration curve. VOCs were analyzed using thermal desorption (Unity2, Markes International, Ltd., Bridgend, UK) gas chromatography (GC) (7890A, Agilent, Santa Clara, CA, USA) mass spectrometry (MS) (5975C, Agilent, Santa Clara, CA, USA), and the analysis method was US EPA TO-17 (solid adsorption method). The 33 compounds used for the analysis included benzene, toluene, ethylbenzene, and xylene both for agricultural chemical analyses and orchard ambient analyses. Briefly, 1 μL of a diluted solution was collected by mixing two standard VOCs in the solid adsorption tube using nitrogen gas at a flow rate of 50 mL/min. In addition, 1 μL of chlorobenzene-d5 at the concentration of 50 mg/L was injected into the adsorption tube, with all the samples at a flow rate of 50 mL/min, using nitrogen gas to finalize the calibration curve. The detailed analytical procedure can be found elsewhere [15].

2.4. Back-Trajectory Analysis of Meteorological and Satellite Data

To identify the source area of long-range transport air parcels, a concentration weighted trajectory (CWT) was applied with CO and CO_2. Backward trajectories arriving in the sampling area were obtained using the HYSPLIT model with GDAS1 meteorological data. To further perform CWT analysis, 120 h backward trajectories that arrived at 1000 m above ground level (AGL) were used. CWT with CO/CO_2 ratio was calculated as follows [16,17]:

$$C_{ij} = \frac{\sum_{n=1}^{k} C_n t_{ijn}}{\sum_{n=1}^{k} t_{ijn}} \tag{1}$$

where C_{ij} was the average ratio of grid ij; k was the total number of concentrations and trajectories; C_n was the hourly CO/CO_2 ratio (ppb/ppm); and t_{ijn} was the residence time of the trajectory through grid ij. The trajectory distribution grid had a $1.0° \times 1.0°$ resolution and a boundary of 110–140° E and 25–50° E.

Data from satellites and meteorology were analyzed during the long-range transport (LRT) period. Aerosol optical depth (AOD) of Terra and Aqua/MODIS and CO Column of Sentinel-5P/TROPOMI were used as satellite data [18–20]. Data passing through the Korean peninsula satellite orbit during the LRT period were calculated using the arithmetic mean [21]. Data on wind direction and speed in 850 hPa from ERA5 were used as meteorological data in this study. ERA5 data were calculated using the arithmetic mean every three hours during the LRT event period to indicate an overall current pattern of Northeast Asia. During the measurement period, MOD04/MYD04 satellite data were used. This parameter data was named "Optical_Depth_Land_And_Ocean". An average MODIS was shown with an arithmetic mean after rearranging 0.25 degrees of spacing grids.

3. Results

3.1. Time Series Results of Measured Concentrations

Table 1 shows the averaged concentrations during the study period. The $PM_{2.5}$ concentration was 21.87 μg/m^3, meaning that it was observed at less than 25.00 μg/m^3 of its Korea Environmental Standard. $PM_{2.5}$ compositions accounted for 80.10% of the total $PM_{2.5}$, including 24.09% carbons of OC and EC, 49.34% ions of SO_4^{2-} and NO_3^-, and 6.63% trace elements. Based on results of previous studies, it was presumed that 19.90%

of compositions except OC, EC, ions, and metals consisted of H, N, S, and O (which are organic matter except for carbon), unmeasured metals, and a small amount of water [4–6]. Gaseous compounds measured in the study area had seven compositions including CO, CO_2, SO_2, O_3, NO, NO_2, and NH_3 at average concentrations of 202.18 ppb, 446.74 ppm, 4.95 ppb, 38.14 ppb, 0.95 ppb, 3.77 ppb, and 6.97 ppb, respectively.

Table 1. Chemical concentration results in the orchard area.

	Compound	Unit	Overall Average	LRT [1] Period	Other Periods	Ratio [2]
Gas	CO	ppb	202.175	283.010	184.521	1.534
	CO_2	ppm	446.742	452.842	445.410	1.017
	SO_2	ppb	4.953	4.823	4.981	0.968
	O_3	ppb	38.140	42.254	37.241	1.135
	NO	ppb	0.950	0.994	0.940	1.058
	NO_2	ppb	3.770	4.957	3.510	1.412
	NH_3	ppb	6.974	14.748	5.366	2.749
PM$_{2.5}$	PM$_{2.5}$	$\mu g/m^3$	21.869	50.863	15.388	3.305
	eBC	$\mu g/m^3$	0.916	1.943	0.692	2.807
	PM$_{2.5}$sum	$\mu g/m^3$	17.499	41.545	11.995	3.464
	OC	$\mu g/m^3$	4.816	7.577	4.184	1.811
	EC	$\mu g/m^3$	0.453	0.789	0.376	2.101
	WSOC	$\mu g/m^3$	3.186	5.239	2.716	1.929
	NO_3^-	$\mu g/m^3$	5.149	17.172	2.397	7.163
	SO_4^{2-}	$\mu g/m^3$	2.754	5.928	2.028	2.923
	NH_4^+	$\mu g/m^3$	2.452	6.821	1.452	4.696
	K+	$\mu g/m^3$	0.086	0.199	0.061	3.277
	Na	$\mu g/m^3$	0.278	0.418	0.247	1.691
	Mg	$\mu g/m^3$	0.077	0.115	0.068	1.688
	Al	$\mu g/m^3$	0.178	0.251	0.162	1.546
	Si	$\mu g/m^3$	0.351	0.495	0.319	1.553
	Cl	$\mu g/m^3$	0.337	0.736	0.250	2.939
	K	$\mu g/m^3$	0.253	0.520	0.194	2.679
	Ca	$\mu g/m^3$	0.113	0.182	0.098	1.844
	Ti	$\mu g/m^3$	0.011	0.016	0.010	1.641
	Cr	$\mu g/m^3$	0.002	0.003	0.002	1.252
	Mn	$\mu g/m^3$	0.011	0.019	0.009	2.140
	Fe	$\mu g/m^3$	0.160	0.244	0.142	1.719
	Ni	$\mu g/m^3$	0.003	0.003	0.003	1.245
	Cu	$\mu g/m^3$	0.001	0.001	0.000	2.555
	Zn	$\mu g/m^3$	0.020	0.038	0.016	2.421
	Br	$\mu g/m^3$	0.003	0.006	0.002	2.340
	Pb	$\mu g/m^3$	0.008	0.014	0.007	1.978

[1] Long-range transport; [2] ratio of long-range transport to other periods.

The characteristic of the study area was investigated using the PM$_{2.5}$ compositions. OC can be divided into water-insoluble organic carbon (WIOC) and water-soluble organic carbon (WSOC). WIOC is mainly generated through the combustion of fossil fuels as a primary origin, and WSOC is released as the primary particulate from sources of biomass burning (BB) or generated by creating a secondary organic aerosol (SOA) [22–26]. WSOC and WIOC accounted for 66% and 34% of the total OC in the study area, respectively. Considering that the study area was located in an agricultural site and the sampling period was in the winter season, it was presumed that WIOC was caused by the use of fossil fuels for heating in winter and that WSOC was caused by biomass burning and SOA formation. From these data, the ratios of K^+/EC and K^+/Cl, which are indicators of biological combustion, were inspected to understand the reason for WSOC. According to previous studies, the ratio of K^+/EC generated by biomass combustion is >2.25 for soft plants such as rice straws, 1~2 for corn, and >0.19 for hard plants such as wood [27–30]. In

addition, the ratio of K^+/Cl generated by biomass combustion is 0.3~1 for crops and 2.8~5.4 for wood [28,31]. In this study, the ratios of K^+/EC and K^+/Cl were 0.19 and 0.26 lower than those of previous studies, respectively. The average ratio of K^+/K in this study was 0.34. Thus, a large amount of K was present in water-insoluble materials. Its origin could be from soils rather than biomass combustion, as reported in previous studies (geological origin of 0.1 for K^+/K, biomass combustion of 0.9 for K^+/K) [28,32]. Meanwhile, the biological combustion of agricultural byproducts in Korea is performed during November and December after completing crop harvests. Thus, the period of this study was set to be from January to February. Based on the results reported above, WSOC might have a bigger influence due to SOA generations than biomass combustions.

Water-soluble ionic compounds accounted for 49.34% of $PM_{2.5}$ compositions, which were the highest. The concentrations of ionic compounds were: 2.452 $\mu g/m^3$ for NH_4^+, 5.149 $\mu g/m^3$ for NO_3^-, 2.754 $\mu g/m^3$ for SO_4^{2-}, and 0.086 $\mu g/m^3$ for K^+. NH_3 in the atmosphere is an alkaline gas that can form ammonium sulfate ($(NH_4)_2SO_4$) or ammonium bisulfate ($(NH_4)HSO_4$) after it is neutralized by sulfuric acid (H_2SO_4). Some NH_3 can form ammonium nitrate (NH_4NO_3) by reacting with nitric acid (HNO_3) [33,34]. Ammonium sulfate, ammonium bisulfate, and ammonium nitrate are all SOAs. Their generations are dominated by NH_3 in the atmosphere. The content of NH_3 was analyzed using the mole ratio of NO_3^-, SO_4^{2-}, and NH_4^+ in $PM_{2.5}$. According to previous studies, the air can be defined as ammonium-rich if the mole ratio of NH_4^+/SO_4^{2-} in $PM_{2.5}$ is higher than 1.5 [35,36]. If the mole ratio of NH_4^+/SO_4^{2-} in $PM_{2.5}$ is lower than 1.5, it is regarded that the contribution of SO_4^{2-} to SOA in $PM_{2.5}$ is significant. When the mole ratio of NO_3^-/SO_4^{2-} is high, the contribution of NO_3^- to SOA is dominant. Thus, the air can be defined as ammonium-rich. In this study, mole ratios of NH_4^+/SO_4^{2-} and NO_3^-/SO_4^{2-} were 4.75 and 2.90, respectively [37,38]. Therefore, NH_4^+ in the atmosphere was sufficient in the study area, and the generation of SOA would be relatively easy due to the high contributions of NO_3^- to SOA. Based on the results of WSOC, water-soluble ions, the ratio of K^+/K, EC, and eBC, $PM_{2.5}$ had the following main causes: SOA generation, combustion of fossil fuels for heating, scattering of earth crustal materials, and so on. However, because WSOC and water-soluble ions accounted for 15.84% and 49.34% of total $PM_{2.5}$, respectively, it could be judged that SOA contributed to $PM_{2.5}$ the most in the study area.

Figure 2 shows wind direction/speed and time-series concentrations. As shown in the graph, the temperature was −11~12 °C during the measurement period, and the relative humidity (RH) was 20~88%. From the measured concentrations, a gaseous material had a 7.55 times difference between minimum and maximum concentrations, and the average $PM_{2.5}$ had a 55.69 times difference between minimum and maximum concentrations. Even within the short period of this study, this displayed a significant difference between compositions of gaseous materials and $PM_{2.5}$. From results shown in Figure 2, significant differences in $PM_{2.5}$ were found during the following periods: 1 p.m. on 30 January~3 p.m. on 31 January, 9 a.m. on 1 February~3 p.m. on 2 February, and 9 a.m. on 6 Feburary~3 p.m. on 7 February. The changes in concentrations during the above periods (event periods) might have been caused by external influxes due to several reasons. The first reason is that the CO concentration increased during the event period. The lifetime of atmospheric CO is about three months in winter. CO is normally an inert precursor for long-range transport for less than 10 days [39]. In addition, because CO reacts with OH radicals in photochemical reactions and produces CO_2, it is known that its daily concentration is very low from 1 p.m. to 4 p.m. when photochemical reactions are definitely active [35,36]. In this study, CO concentrations during the event period and other periods were 283 ppb and 184 ppb, respectively, showing a higher concentration during the event period. CO concentrations by time indicated that its average concentration was about 180 ppb from 6 a.m. to 9 a.m. and about 150 ppb from 1 p.m. to 4 p.m. during other periods, showing lower concentrations when photochemical reactions were occurring. On the other hand, its concentration during the event period was 220 ppb from 6 a.m. to 9 a.m. and 270 ppb from 1 p.m. to 4 p.m. when photochemical reactions were dominating. Based on daily

concentration changes in CO and CO concentrations by time at the event period and other periods, the study area might be affected by external influxes during the event period. The second reason is the increase in EC during the event period. According to previous studies, an increase in EC could result from external influxes if no specific EC sources are available. A 68% increase in EC has been reported [40]. Our study location was an orchard located in an agricultural region without any residential houses, highways, or industrial duplexes discharging EC nearby. However, EC was found to be increased about 2.1 times when comparing its concentrations between the event period and other periods. This increase in EC during the event period might be due to external influxes associated with the geological features of the study location. The third reason for an external influx is that water-soluble ions were the main cause of increased $PM_{2.5}$. Previous studies have insisted that an increase in SOA is a big factor influencing long-range transport [40]. Generally, atmospheric SO_2 and NO_2 react with hydroxyl radicals and generate sulfuric acid and nitric acid. Then nano-particles such as $(NH_4)_2SO_4$, $(NH_4)HSO_4$, and NH_4NO_3 are produced by reactions between ammonia and sulfuric and nitric acids [41,42].
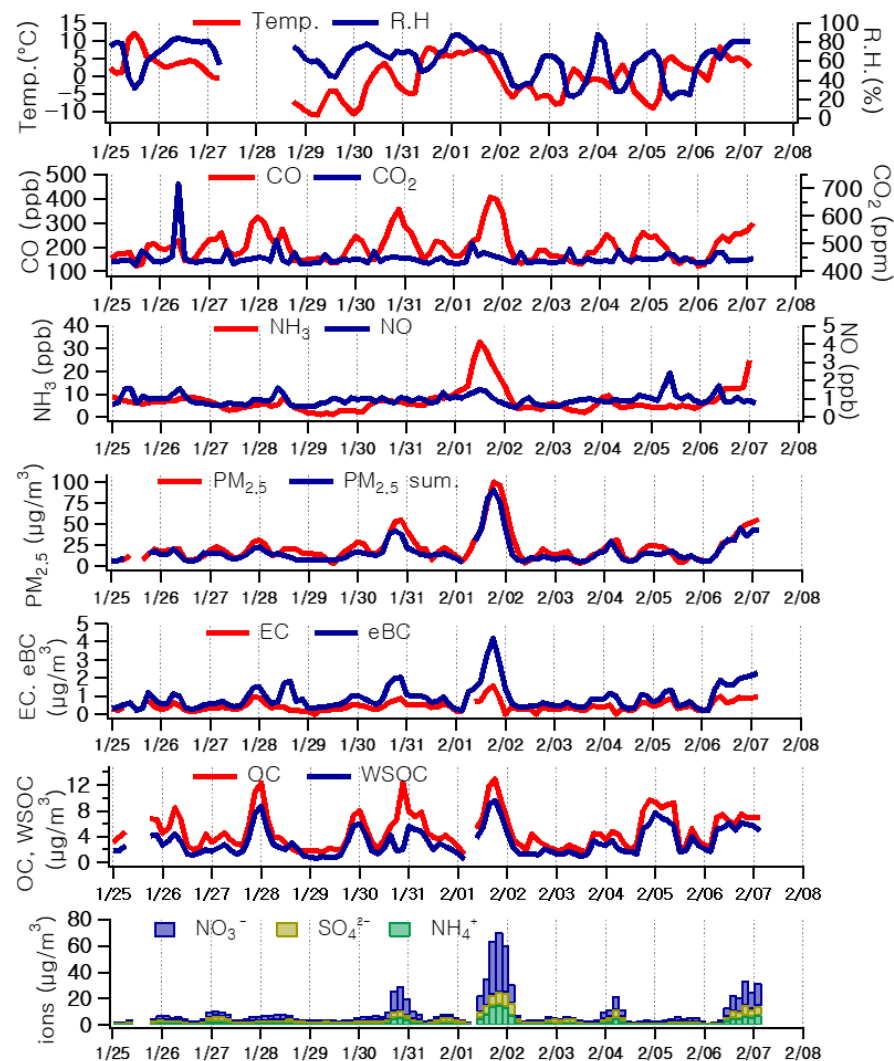
Figure 2. Time-series concentrations of $PM_{2.5}$, CO, CO_2, EC, eBC, and ionic compounds.

Additionally, if ammonia is available after NH_3 reacts with sulfuric acid first, it can react with nitric acid [31]. This study showed that the content of water-soluble ions within $PM_{2.5}$ was 60.27% during the event period and 40.64% during other periods. Thus, the event period had a higher content of water-soluble ions than other periods. Concentrations of SO_4^{2-}, NO_3^{-}, and NH_4^{+} within $PM_{2.5}$ were increased about 2.9 times, 7.2 times, and

4.7 times, respectively, during the event period compared with those during other periods. On the other hand, atmospheric concentrations of SO_2, NO, and NO_2 (factors to generate SOA such as SO_4^{2-} and NO_3^-) in $PM_{2.5}$ were increased by 0.97 times, 1.06 times, and 1.4 times, respectively. Their increases were much lower than the increases in water-soluble ions in $PM_{2.5}$. Along with ammonium-rich SOA due to NO_3^-, SO_4^{2-}, and NH_4^+, the mole ratio of NH_4^+/SO_4^{2-} was 3.8 during other periods and 6.14 during the event period, indicating a stronger condition for SOA during the event period than during other periods. Based on the mole ratio of NO_3^-/SO_4^{2-}, the contribution of NO_3^- to $PM_{2.5}$ was also higher during the event period, which was 4.5 compared with 1.83 during other periods. Atmospheric NH_3, a dominant factor for generating SOA by NO_3^-, SO_4^{2-}, and NH_4^+, displayed about a 2.7 times difference between the event period and other periods. There were small differences in concentrations of SO_2, NO, and NO_2 during each period. Even without increasing concentrations of SO_2, NO, and NO_2 in the atmosphere, these materials could be caused by external influxes such as an increase in water-soluble ions like NO_3^-, SO_4^{2-}, and NH_4^+ in $PM_{2.5}$, ammonium-rich status increase during the event period, and increased contributions of NO_3^- and gaseous NH_3. That is, types of water-soluble ion compounds were increased during the event period. After sufficient NH_3 in the process of SOA formation reacted with sulfuric and nitric acids, the remaining NH_3 might affect the study area. Some previous studies have suggested that an increase in NH_3 is due to external influxes and that SOA compositions in $PM_{2.5}$ and NH_3 can be increased by long-range transport. External influxes can be classified into three types based on distance, including short distances (less than 100 Km), medium distances (100~550 Km), and long distances (longer than 550 Km). It has been shown that an external influx with an SOA increase is generated by medium and long distances [40].

3.2. Satellite Observations for Long-Range Transport

To identify the external influx into the study area, we looked over the results of satellite observations provided in aerosol optical depth (AOD), ERA wind field during the event period, back-trajectory analysis, and Sentinel for CO/CO_2. Because AOD provides information on the relative weights of pollutants existing in the atmospheric column, it is useful to investigate changes in spatial contributions for particulates. AOD uses MOD04/MYD04 data from TERRA, a representative satellite, to observe the Earth. MODIS sensor observation data are loaded on the Aqua satellite. All data that corresponded to the event period were rearranged into 0.25-degree grids after obtaining arithmetic means. However, we could not obtain all data during the entire event period due to orbit limitations of the Terra and Aqua satellites, and thus the results were calculated using data from 12 p.m. to 2 p.m. on 30 January, 10 a.m. to 2 p.m. on 1 February, and 11 a.m. to 4 p.m. on 6 February. Figure 3 shows the observation data for AOD. As shown in this graph, AOD had a wide range of 0.7~1.4 from West China centered in Shanghai, China, to the study area.
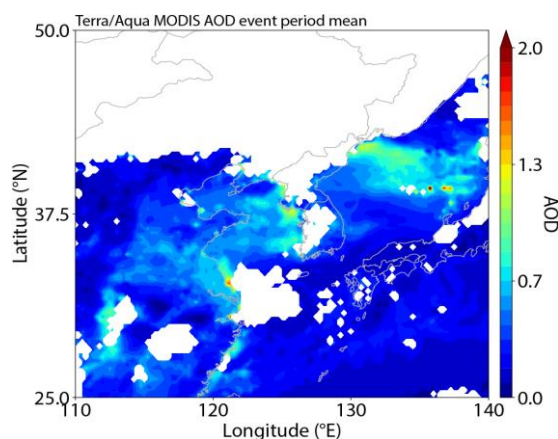
Figure 3. Levels of aerosols in the area at the average of the event periods in AOD satellite observation.

Data from Sentinel-5 Precursor (S-5 P) observed during the study period were confirmed. S-5 P is a satellite with a single fade is used in GMES (Global Monitoring for Environment and Security) that is operated by the EU community and the European Space Agency for common goals [18]. To provide high-quality data, information, service, and knowledge in time, GMES aims to support European goals for sustainable development and environmental global governance. S-5 P provides daily information for air quality and concentrations of trace gases and aerosols that are important for climate forcing and ozone. In detail, S-5 P observes air quality using TROPOMI (tropospheric monitoring instrument, co-developed by the Netherlands and European Space Agency) and a spectrometer having spectrum bands of UV, visible light (VIS), near-infrared (NIR), and short wavelength infrared (SWIR). Major atmospheric components such as O_3, NO_2, CO, SO_2, methane (CH_4), formaldehyde (CH_2O), aerosols, and clouds can be observed using selected wavelength ranges in TROPOMI [43]. Thus, analyzed CO from data from S-5 P observed during the period of this study. Figure 4 indicates the concentration gradient of CO observed by S-5 P. As shown in the figure, CO appeared in high concentrations in China. High levels of CO from the study area to Japan were also confirmed.
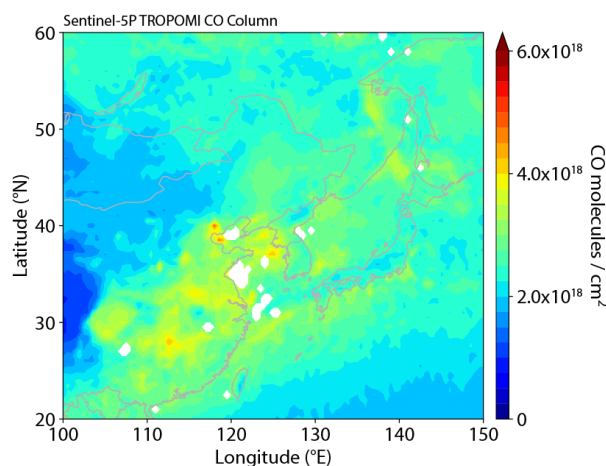
Figure 4. The concentration gradient in CO observed by S-5P.

Figure 5 shows data from the ERA wind field and meteorological field. We illustrated the ERA wind field and meteorological field on the same map of the back-trajectory graph using the U and V components of ERA5 data provided by the European Centre for Medium-Range Weather Forecasts (ECMWF). These data confirmed that the study area was influenced by the west wind from China on 30 January, 1~2 February, and 6~7 February.

A back-trajectory analysis was performed using the ratio of CO/CO_2 to confirm the external influx in the study area. The reason why the ratio of CO/CO_2 was used for the back-trajectory analysis is because CO can be used as an inert precursor for long-range transport. In addition, it is a gaseous material that showed a high concentration during the event period, which can be estimated during the period of external influx. Its concentration in the study area only showed a 1.01 times difference between the event period and other periods. Thus, the ratio of CO/CO_2 can be used as a marker for external influxes. In this study, the residence time-weighted concentration (RTWC) model was used for the back-trajectory analysis. By complementing the disadvantages of the potential source contribution function (PSCF) model, the RTWC model can impose a weighted concentration by the source on each grid for calculating each average concentration of grid cells. In detail, the PSCF model can indicate the possibility of arriving at a detention place after a component with some pollutants passes through the source by a specific wind. However, it has a disadvantage in that it cannot apply concentration weight by time because movements of sources are generated by the same retention time even when source materials have some concentration differences [44–47]. The RTWC model can impose a weighted concentration by the source,

thus overcoming the disadvantage of the PSCF model. Figure 6 shows the results of the RTWC model realized for the ratio of CO/CO_2 during the total study period. It does not display the actual contribution because its concentration of RTWC by area is expanded by the number of trajectory segments whenever concentrations are distributed in each grid cell [46]. Therefore, it is difficult to understand the actual concentration by area with the concentrations shown in the figure only. However, the RTWC model suggests a relative importance of source locations measured in the study area [46]. In the case of interpreting the relative importance of source locations, the ratio of CO/CO_2 was introduced from the west and northwest of the study area. A similar result for the wind field was found, as shown in Figure 6.
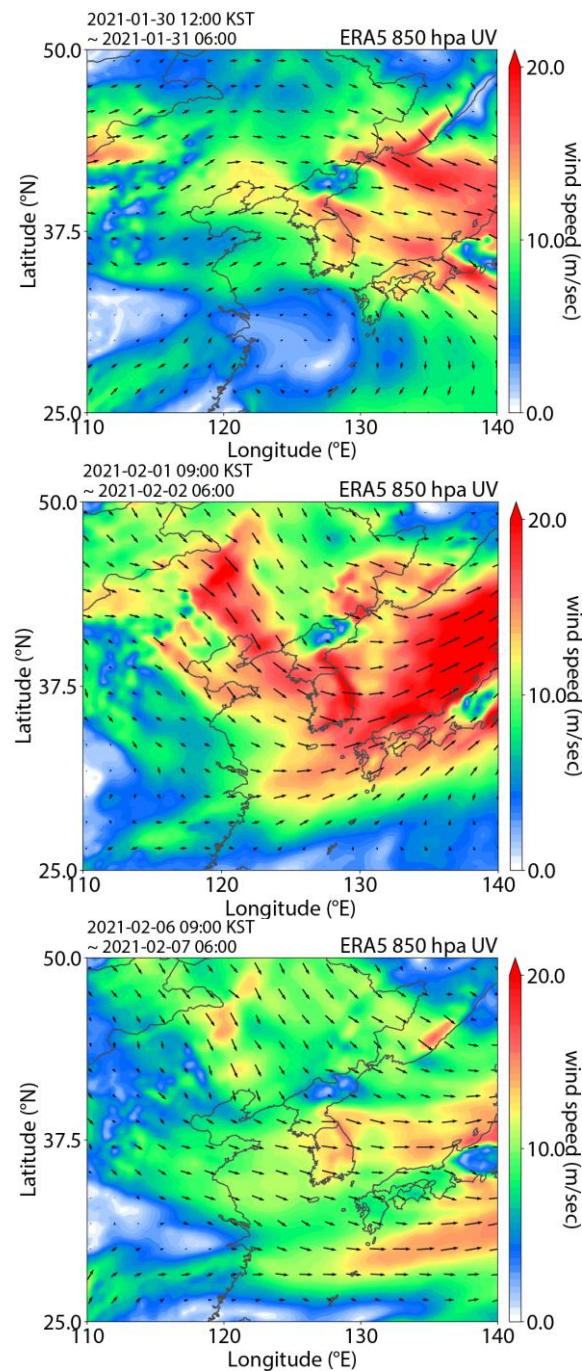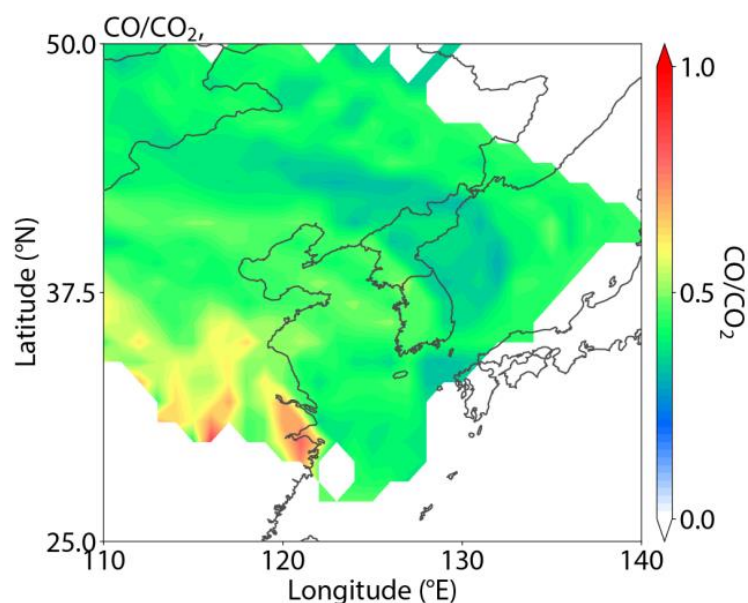

Figure 5. ERA Wind Field and Meteorological Field Data (European ECMWF).

Figure 6. The ratio of CO and CO_2 and the result of the residence time-weighted concentration (RTWC) model in the study area.

As a result of identifying external influxes in the study area and analyzing data from AOD and S-5 P, high concentrations of aerosol and CO from China (west of the study area) and ERA wind fields flowing from the west and northwest of the study area were confirmed. Additionally, the ratio of CO/CO_2 from the RTWC model had an external influence from the same direction as the ERA wind field. Conclusively, results of back-trajectory analysis using AOD, S-5 P, ERA wind field, and RTWC confirmed that external influxes during the event period affected the study area.

3.3. Ratio Characteristic of Long-Range Transport Component

Based on the chemical compositions of $PM_{2.5}$, AOD, S-5 P, RTWC, and the ERA wind field during the event period in this study, it can be concluded that a high concentration of $PM_{2.5}$ generated by long-range transport from the west of the study area had external effects. Thus, this study identified precursor components for long-range transport based on concentration differences between the event period and other periods. Chemical compounds that influenced the event period were selected based on concentrations measured during the event period and other periods. The analytical determination was the following: (1) a compound that was observed to show an increase in concentration during the event period; (2) a compound that affected SOA formation; and (3) a compound that satisfied the condition suggested by a previous study as an inert precursor of long-range transport. As a result, the indicators for long-distance tracking included gaseous materials (including CO and NH_3) and $PM_{2.5}$ compositions (such as eBC, EC, WSOC, OC, NO_3^-, SO_4^{2-}, and NH_4^+). Table 2 shows the results for the selected long-range indicators and $PM_{2.5}$. When results were compared between the event period and other periods, $PM_{2.5}$ and gaseous materials including CO and NH_3 were about 3.3 times, 1.5 times, and 2.7 times higher, respectively, during the event period. For $PM_{2.5}$ compositions, NO_3^-, SO_4^{2-}, and NH_4^+ were increased by about 7.16 times, 2.9 times, and 4.7 times, respectively. These results confirmed that the $PM_{2.5}$ concentration increase during the event period was influenced by SOA from long-range transport. In addition, WSOC was influenced by SOA introduced by long-range transport because WSOC had about a 2 times increase during the event period and a dominant effect on SOA formation.

Table 2. Concentrations of tracer components for long-range transport.

	Compound	Unit	Overall Average	LRT [1] Periods	Other Periods	Ratio [2]
Gas	CO	ppb	202.175	283.010	184.521	1.534
	NH_3	ppb	6.974	14.748	5.366	2.749
$PM_{2.5}$	$PM_{2.5}$ mass	$\mu g/m^3$	21.869	50.863	15.388	3.305
	eBC	$\mu g/m^3$	0.916	1.943	0.692	2.807
	OC	$\mu g/m^3$	4.816	7.577	4.184	1.811
	EC	$\mu g/m^3$	0.453	0.789	0.376	2.101
	WSOC	$\mu g/m^3$	3.186	5.239	2.716	1.929
	NO_3^-	$\mu g/m^3$	5.149	17.172	2.397	7.163
	SO_4^{2-}	$\mu g/m^3$	2.754	5.928	2.028	2.923
	NH_4^+	$\mu g/m^3$	2.452	6.821	1.452	4.696

[1] Long-range transport; [2] ratio of long-range transport to other periods.

Among the $PM_{2.5}$ components, eBC and EC were compared between the event period and other periods. eBC and EC are primarily derived from the combustion of fossil fuels and incomplete combustion of biomass. Regarding their analytical methods, EC can be determined using the thermo-optical method, and eBC can be determined using optical technology [48,49]. In the case of eBC/EC with the NIOSH5040 protocol, $PM_{2.5}$ was generally in the range of 1.4~1.7. It might have a maximum difference of two times depending on particle size distribution, mixing status, and chemical compositions [50–52]. Except for the difference in analytical methods between eBC and EC, there are two examples that show differences between eBC and EC. The first is that brown carbon generated by biomass combustion increases eBC more than EC [53,54]. The second is an underestimation of EC using char-OC, which is contained in samples. Previous studies have reported that methanol extraction of char-OC contained within filters can increase EC by more than two times [49,55]. In other words, char-OC within filters can cause an underestimation of EC and an increase in the eBC/EC ratio. The measured ratio of eBC/EC in this study was 2.02 during other periods and 2.46 during the event period. Study areas specified by ratios of K^+/K and K^+/Cl had relatively low combustions of biomass. The orchard did not have any sources generating char-OC. Thus, the eBC/EC increase during the event period should be due to external influxes.

To evaluate the above results more accurately, we analyzed correlations between CO and CO_2 and SOA formation indicators including SO_4^{2-}, NO_3^-, NH_4^+ (SNA), eBC, and EC (Figure 7). Regarding the correlation between CO and CO_2, CO_2 displayed a relatively homogenous concentration throughout the study period. However, CO concentration was obviously increased during the event period. That is, the increasing rate of CO as an origin of CO_2 was not related to the CO_2 increase during the event period, meaning that the ratio of CO/CO_2 could be used as an indicator for external influxes. To examine SOA inflow by SNA, we examined the correlation between $[NO_3^-/SO_4^{2-}]$ and $[NH_4^+/SO_4^{2-}]$ and the correlation between NH_3 and NO. Figure 7 shows a linear relationship between $[NO_3^-/SO_4^{2-}]$ and $[NO_4^+/SO_4^{2-}]$. Meanwhile, it was confirmed that NH_3 increased more than NO during the event period. In $PM_{2.5}$ compositions, $PM_{2.5}$ introduced during the event period flowed into the study area in a type of SOA based on SNA. However, NO_2 and SO_2 were not introduced in gas states because they completely reacted with NH_3. On the other hand, it was confirmed that the remaining NH_3 was introduced into the study area after reacting with atmospheric NO_2 and SO_2. Therefore, a linear relationship between $[NO_3^-/SO_4^{2-}]$ and $[NH_4^+/SO_4^{2-}]$ in $PM_{2.5}$ could play a role as an indicator that NH_3/NO increases atmospheric NH_3 due to external influxes. The correlation between eBC and EC during the event period also showed a linear proportional relationship, with an eBC/EC ratio of approximately 2.0. It was hard to evaluate external influxes based on the ratio of eBC to EC. However, when data on 28 January and 1 February, which had strong external influxes during the event period, were analyzed, the ratio of eBC/EC could be used as an evaluation index for strong external influxes because it increased from 2.0 to 2.4 or higher.
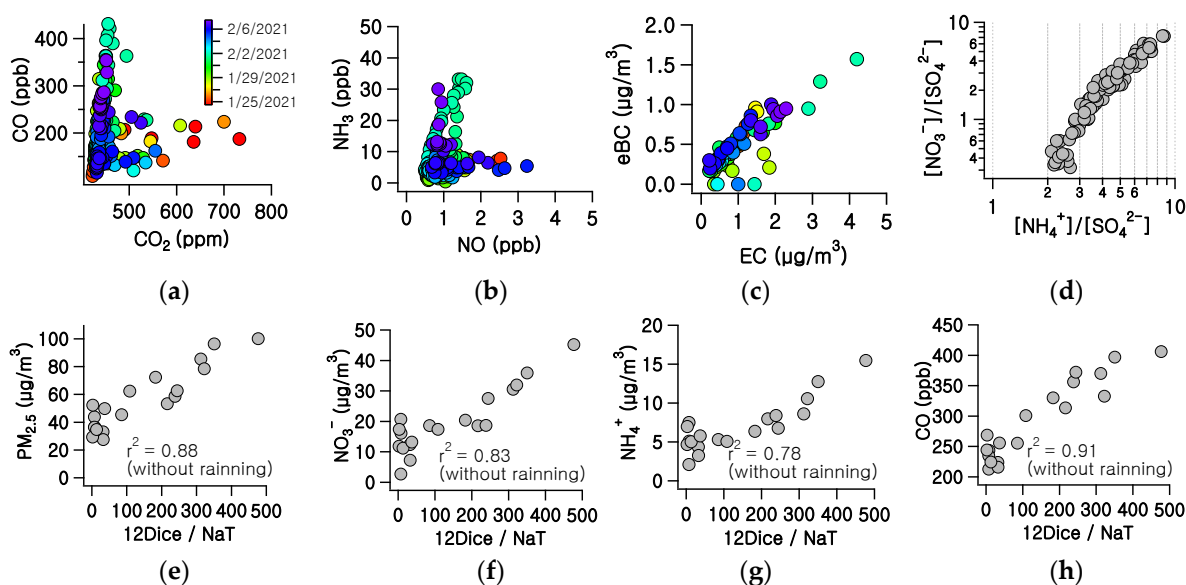
Figure 7. Scatter plots between (**a**) CO and CO_2, (**b**) NH_3 and NO, (**c**) eBC and EC, (**d**) $[NO_3^-/SO_4^{2-}]$ and $[NH_4^+/SO_4^{2-}]$, (**e**) $PM_{2.5}$ and 12Dice/Nat, (**f**) NO_3^- and 12Dice/Nat, (**g**) NH_4^+ and 12Dice/Nat, and (**h**) CO and 12Dice/Nat.

3.4. Long-Distance Transport Using VOCs

We then determined whether the 32 VOCs measured in this study could be used as an evaluation index for long-range transport. It is well known that VOCs are generally removed by the physical adsorption process of wet and dry deposition in the troposphere and transformed by photolysis and OH radical reactions [56]. Adsorption removal of VOCs in wet and dry environments is determined by temperature, humidity, and pressure in the troposphere. The change in VOCs is influenced by oxidation speed for OH radicals. This oxidation speed for OH radical is different in VOC compounds involved in the lifetime of VOCs [57]. According to a previous study, K_{OH} values of m-xylene and p-xylene are 23.6 and 14.3, respectively. The lifetime of m-xylene and p-xylene in the air are 11.8 h and 19.4 h, respectively. K_{OH} and the lifetime of ethylbenzene are 6.05 and 1.6 days, respectively [57]. These data were used as an evaluation index for long-range transport in this study using VOC lifetime in the air and components that increased during the event period.

Table 3 indicates concentrations of VOCs in this study. The average VOC concentration during the total study period was 2.588 ppb, including 2.118 ppb during the event period and 2.682 ppb during other periods. The concentrations of VOCs were about 22% lower during the event period than during other periods. However, the concentrations were higher during the event period than during other periods for chloroform (Cf), 1,2-dichloroethane (12Dice), tetrachloroethene (TcCE), and chlorobenzene (CB). For comparisons between the event and other periods, the concentrations of Cf, 12Dice, TcCE, and CB were found to be 1.92 times, 3.74 times, 1.67 times, and 2.00 times higher, respectively, during the event period. Considering the four VOCs mentioned above, previous studies indicate that Cf, 12Dice, TcCE, and CB have a lifetime in the air of 146 days, 90 days, 200 days, and 13 days, respectively [58–60]. In addition, the time for VOCs to arrive at the study area was 12~48 h based on the back-trajectory analysis. Thus, Cf, 12Dice, TcCE, and CB might have been introduced into the study area by long-range transport based on the overall concentration increases, lifetime in the air, and arrival time calculated using the back-trajectory analysis during the event period.

Table 3. VOCs concentrations measured during the study period.

Compound [1]	Overall Average	LRT [2] Periods	Other Periods	Ratio [3]	Non Event STD [4]
Acrylonitrile	0.021	0.016	0.022	0.727	0.029
1,1-Dichloroethane	0.234	0.266	0.221	1.204	0.289
Chloroform	0.045	0.075	0.039	1.923	0.041
1,2-Dichloroethane	0.044	0.116	0.031	3.742	0.025
Benzene	0.729	0.483	0.781	0.618	0.782
Carbon tetrachloride	0.048	0.044	0.049	0.898	0.018
Trichloroethene	0.007	0.004	0.008	0.500	0.017
Toluene	0.986	0.677	1.052	0.644	1.699
Tetrachloroethene	0.006	0.010	0.006	1.667	0.007
Chlorobenzene	0.007	0.012	0.006	2.000	0.012
Ethylbenzene	0.100	0.098	0.101	0.970	0.166
m&p-Xylene	0.040	0.042	0.040	1.050	0.079
Styrene	0.080	0.060	0.084	0.714	0.057
o-Xylene	0.047	0.045	0.047	0.957	0.078
Bromobenzene	0.051	0.035	0.053	0.660	0.067
Isopropylbenzene	0.007	0.007	0.007	1.000	0.006
2-Chlorotoluene	0.002	0.001	0.002	0.500	0.004
1,3,5-Trimethylbenzene	0.004	0.003	0.004	0.750	0.004
p-Isopropylbenzene	0.010	0.011	0.009	1.222	0.010
1,2,4-Trimethylbenzene	0.017	0.018	0.017	1.059	0.007
1,2-DiChlorobenzene	0.004	0.004	0.004	1.000	0.002
1,3-DiChlorobenzene	0.001	0.001	-	-	0.002
tert-Butylbenzene	0.001	-	0.001	-	0.002
1,4-DiChlorobenzene	-	0.001	-	-	0.001
n-Butylbenzene	0.007	0.007	0.007	1.000	0.003
Naphthalene	0.090	0.082	0.091	0.901	0.014
∑VOCs	2.588	2.118	2.682		

[1] Unit: ppb; [2] long-range transport; [3] ratio of long-range transport to other periods; [4] standard deviation.

Cf, 12Dice, TcCE, and CB transported into the study area by long-range transport can be released artificially or naturally [61]. It is particularly difficult to investigate natural and artificial sources of Cf. In addition, CB is an ingredient of pesticides [60,61]. The study area was an orchard located in an agricultural region. Only comparing concentrations between events and other periods is not enough to evaluate external influxes due to the natural generation of VOCs and the frequent usage of pesticides. Therefore, concentrations of Cf, 12Dice, TcCE, CB, and naphthalene (NaT) during the event period were determined in this study. The reason for selecting NaT is because NaT, in an artificial atmospheric environment, is evaluated as the most abundant component of PAHs and that gaseous NaT is eliminated in a short time [62]. A previous study indicated that its lifetime in the air is 48 min~9 h with the OH radical, according to specific circumstances [62]. Therefore, it is expected that NaT will disappear within 12 h, which is the minimum time for an external influx. As indicated in Table 3, the deviation in NaT concentration during other periods was very low at 0.014. This means that gaseous NaT was abundantly distributed in the atmospheric environment. It is a compound with a short lifetime and a relatively low deviation in the study area. Ratios of Cf, 12Dice, TcCE, and CB to NaT were 2.047 times, 3.967 times, 2.005 times, and 1.974 times higher during the event period than during other periods, respectively. These results confirmed that concentrations of Cf, 12Dice, TcCE, and CB were increased not by emission sources in the study area but by external influxes.

Table 4 and Figure 7 show relationships between Cf/NaT, 12Dice/NaT, TcCE/NaT, and CB/NaT and CO, eBC, EC, OC, WSOC, NH_4^+, NO_3^-, and $PM_{2.5}$ during the event period. As indicated in the table, r^2 for Cf/NaT, 12Dice/NaT, TcCE/NaT, and CB/NaT were 0.170, 0.783, 0.507, and 0.568, respectively. This means that Cf/NaT had no relationship with long-range transport. However, TcCE/NaT and CB/NaT were partially related to

long-range transport. Meanwhile, 12Dice/NaT presented a high correlation with long-range transport. Thus, 12Dice can be used as an indicator for long-range transport. Because the r^2 of CO and 12Dice/NaT, as a direct index for long-range transport, was higher than 0.9, 12Dice/NaT can be used as an indicator for long-range transport with CO/CO_2.

Table 4. Correlation coefficient of determinations between VOC ratios for long-range transport and measured compounds.

r^2	Cf/NaT	12Dice/NaT	TcCE/NaT	CB/NaT
$PM_{2.5}$	0.323	0.879	0.382	0.505
CO	0.321	0.907	0.436	0.525
eBC	0.084	0.792	0.630	0.663
EC	0.026	0.610	0.610	0.609
OC	0.104	0.783	0.629	0.641
WSOC	0.101	0.647	0.442	0.509
NH_4^+	0.220	0.780	0.409	0.504
NO_3^-	0.180	0.834	0.519	0.585

These results clarified the possibility of using VOCs as an indicator for long-range transport. It was confirmed that 12Dice could be used as an evaluation index for long-range transport based on the overall results of VOC lifetime in the air, increases during event period, and correlations with other long-distance indices.

4. Conclusions

This study investigated the influence of long-range transport as one of the $PM_{2.5}$ factors in agricultural regions and estimated an indicator of long-range transport. There was an influence of long-range transport during the observation period. Concentrations of gaseous materials and PM compositions were inspected to find proof of long-range transport. The obtain results imply long-range transport based on changes in gas concentrations and PM compositions. In addition, the AOD, ERA wind field, back-trajectory analysis for CO/CO_2, and satellite observation results were used to identify additional proof for long-range transport. The specific characteristic of long-range transport in the study area during this study was then determined. Long-range transport can be analyzed along with concentrations of CO, NH_3, OC, and water-soluble ions in the future. Furthermore, we confirmed that the ratio of 12Dice/NaT in VOCs had a proportional relationship with an indicator of long-range transport. This suggests that VOCs can be used as markers for long-range transport. Atmospheric pollutants are influenced not only by local factors but also by wide-ranging factors such as intercountry transport. It is hoped that, based on the results presented in this study, a further understanding of the impact of atmospheric pollutants between regions and countries can be achieved, facilitating not only regional atmospheric pollutant management but also global atmospheric pollutant management.

Author Contributions: M.K. and M.S. equally contributed to this work by completing the experiment measurements, data analysis, and manuscript preparation. S.-H.O., G.-H.Y., S.C., H.J. and J.-H.K. contributed to research sample analyses. M.-S.B. contributed to the experimental planning and data analysis. All authors have read and agreed to the published version of the manuscript.

Institutional Review Board Statement: Not applicable.

Informed Consent Statement: Not applicable.

Data Availability Statement: The data will be available upon request.

Conflicts of Interest: The authors declare no conflict of interest.

Abbreviations

The following abbreviations are used in this manuscript:

PM	particulate matter
$PM_{2.5}$	particles that are 2.5 microns or less in diameter
PM_{10}	particles that are 10 microns or less in diameter
VOCs	volatile organic compounds
EC	elemental carbon
OC	organic carbon
WSOC	water soluble organic carbon
MAAP	multi-angle absorption photometer
DDW	deionized distilled water
IC	ion chromatography
TOC	total organic carbon
ED-XRF	energy dispersive X-ray fluorescence
GC	gas chromatography
MS	mass spectrometry
CWT	concentration weighted trajectory
LRT	long-range transport
AOD	aerosol optical depth
WIOC	water insoluble organic carbon
BB	biomass burning
SOA	secondary organic aerosol
RH	relative humidity
VIS	visible light
NIR	near infrared
SWIR	short wavelength infrared
ECMWF	European Centre for Medium-Range Weather Forecasts
RTWC	residence time weighted concentration
PSCF	potential Source Contribution Function
SNA	SO_4^{2-}, NO_3^-, NH_4^+
Cf	chloroform
12Dice	1,2-dichloroethane
TcCE	tetrachloroethene
CB	chlorobenzene
NaT	naphthalene

References

1. Dominici, F.; Peng, R.D.; Bell, M.L.; Pham, L.; McDermott, A.; Zeger, S.L.; Samet, J.M. Fine particulate air pollution and hospital admission for cardiovascular and respiratory diseases. *JAMA* **2006**, *295*, 1127–1134. [CrossRef] [PubMed]
2. Zanobetti, A.; Franklin, M.; Koutrakis, P.; Schwartz, J. Fine particulate air pollution and its components in association with cause-specific emergency admissions. *Environ. Health* **2009**, *8*, 58. [CrossRef] [PubMed]
3. Maji, K.J.; Ye, W.-F.; Arora, M.; Shiva Nagendra, S.M. $PM_{2.5}$-related health and economic loss assessment for 338 Chinese cities. *Environ. Int.* **2018**, *121*, 392–403. [CrossRef] [PubMed]
4. Chow, J.C.; Watson, J.G.; Lowenthal, D.H.; Chen, L.-W.A.; Motallebi, N. Black and Organic Carbon Emission Inventories: Review and Application to California. *J. Air Waste Manag. Assoc.* **2010**, *60*, 497–507. [CrossRef]
5. Gentner, D.R.; Isaacman, G.; Worton, D.R.; Chan, A.W.H.; Dallmann, T.R.; Davis, L.; Goldstein, A.H. Elucidating secondary organic aerosol from diesel and gasoline vehicles through detailed characterization of organic carbon emissions. *Proc. Natl. Acad. Sci. USA* **2012**, *109*, 18318. [CrossRef]
6. Sandrini, S.; Fuzzi, S.; Piazzalunga, A.; Prati, P.; Bonasoni, P.; Cavalli, F.; Gilardoni, S. Spatial and seasonal variability of carbonaceous aerosol across Italy. *Atmos. Environ.* **2014**, *99*, 587–598. [CrossRef]
7. Hellack, B.; Quass, U.; Beuck, H.; Wick, G.; Kuttler, W.; Schins, R.P.; Kuhlbusch, T.A. Elemental composition and radical formation potency of PM_{10} at an urban background station in Germany in relation to origin of air masses. *Atmos. Environ.* **2015**, *105*, 1–6. [CrossRef]
8. Krumpen, T.; Belter, H.J.; Boetius, A.; Damm, E.; Haas, C.; Hendricks, S.; Stein, R. Arctic warming interrupts the Transpolar Drift and affects long-range transport of sea ice and ice-rafted matter. *Sci. Rep.* **2019**, *9*, 5459. [CrossRef]
9. Ryall, D.; Derwent, R.; Manning, A.; Redington, A.; Corden, J.; Millington, W.; Fuller, G. The origin of high particulate concentrations over the United Kingdom, March 2000. *Atmos. Environ.* **2002**, *36*, 1363–1378. [CrossRef]

10. Valenzuela, A.; Olmo, F.; Lyamani, H.; Antón, M.; Quirantes, A.; Alados-Arboledas, L. Classification of aerosol radiative properties during African desert dust intrusions over southeastern Spain by sector origins and cluster analysis. *J. Geophys. Res. Atmos.* **2012**, *117*, D6. [CrossRef]

11. Uygur, N.; Karaca, F.; Alagha, O. Prediction of sources of metal pollution in rainwater in Istanbul, Turkey using factor analysis and long-range transport models. *Atmos. Res.* **2010**, *95*, 55–64. [CrossRef]

12. Choo, G.-H.; Lee, K.; Seo, J.; Kim, S.-Y.; Lee, D.-W.; Shin, H.-J. Optical and chemical properties of long-range transported aerosols using satellite and ground-based observations over seoul; South Korea. *Atmos. Environ.* **2021**, *246*, 118024. [CrossRef]

13. Kim, H.; Zhang, Q.; Heo, J. Influence of intense secondary aerosol formation and long-range transport on aerosol chemistry and properties in the Seoul Metropolitan Area during spring time: Results from KORUS-AQ. *Atmos. Chem. Phys.* **2018**, *18*, 7149–7168. [CrossRef]

14. Thang, P.Q.; Kim, S.-J.; Lee, S.-J.; Ye, J.; Seo, Y.-K.; Baek, S.-O.; Choi, S.-D. Seasonal characteristics of particulate polycyclic aromatic hydrocarbons (PAHs) in a petrochemical and oil refinery industrial area on the west coast of South Korea. *Atmos. Environ.* **2019**, *198*, 398–406. [CrossRef]

15. Song, M.; Kim, M.; Oh, S.; Park, C.; Kim, M.; Kim, M.; Lee, H.; Choe, S.; Bae, M. Influences of Organic Volatile Compounds on the Secondary Organic Carbon of Fine Particulate Matter in the Fruit Tree Area. *Appl. Sci.* **2021**, *11*, 8193. [CrossRef]

16. Cheng, I.; Zhang, L.; Blanchard, P.; Dalziel, J.; Tordon, R. Concentration-weighted trajectory approach to identifying potential sources of speciated atmospheric mercury at an urban coastal site in Nova Scotia, Canada. *Atmos. Chem. Phys.* **2013**, *13*, 6031–6048. [CrossRef]

17. Dimitriou, K.; Kassomenos, P. Aerosol contributions at an urban background site in Eastern Mediterranean–Potential source regions of PAHs in PM_{10} mass. *Sci. Total Environ.* **2017**, *598*, 563–571. [CrossRef]

18. Magro, C.; Nunes, L.; Gonçalves, O.C.; Neng, N.R.; Nogueira, J.M.F.; Rego, F.C.; Vieira, P. Atmospheric Trends of CO and CH_4 from Extreme Wildfires in Portugal Using Sentinel-5P TROPOMI Level-2 Data. *Fire* **2021**, *4*, 25. [CrossRef]

19. Schneising, O.; Buchwitz, M.; Reuter, M.; Bovensmann, H.; Burrows, J.P.; Borsdorff, T.; Wunch, D. A scientific algorithm to simultaneously retrieve carbon monoxide and methane from TROPOMI onboard Sentinel-5 Precursor. *Atmos. Meas. Tech.* **2019**, *12*, 6771–6802. [CrossRef]

20. Tian, X.; Gao, Z. Validation and Accuracy Assessment of MODIS C6.1 Aerosol Products over the Heavy Aerosol Loading Area. *Atmosphere* **2019**, *10*, 548. [CrossRef]

21. Hoffmann, L.; Günther, G.; Li, D.; Stein, O.; Wu, X.; Griessbach, S.; Wright, J.S. From ERA-Interim to ERA5: The considerable impact of ECMWF's next-generation reanalysis on Lagrangian transport simulations. *Atmos. Chem. Phys.* **2019**, *19*, 3097–3124. [CrossRef]

22. Bozzetti, C.; Haddad, I.E.; Salameh, D.; Daellenbach, K.R.; Fermo, P.; Gonzalez, R.; Elser, M. Organic aerosol source apportionment by offline-AMS over a full year in Marseille. *Atmos. Chem. Phys.* **2017**, *17*, 8247–8268. [CrossRef]

23. Miyazaki, Y.; Kondo, Y.; Takegawa, N.; Komazaki, Y.; Fukuda, M.; Kawamura, K.; Weber, R. Time-resolved measurements of water-soluble organic carbon in Tokyo. *J. Geophys. Res. Atmos.* **2006**, *111*, D23. [CrossRef]

24. Sannigrahi, P.; Sullivan, A.P.; Weber, R.J.; Ingall, E.D. Characterization of water-soluble organic carbon in urban atmospheric aerosols using solid-state 13C NMR spectroscopy. *Environ. Sci. Technol.* **2006**, *40*, 666–672. [CrossRef] [PubMed]

25. Weber, R.J.; Sullivan, A.P.; Peltier, R.E.; Russell, A.; Yan, B.; Zheng, M.; Holloway, J.S. A study of secondary organic aerosol formation in the anthropogenic-influenced southeastern United States. *J. Geophys. Res. Atmos.* **2007**, *112*, D13. [CrossRef]

26. Zhang, Y.-L.; Li, J.; Zhang, G.; Zotter, P.; Huang, R.-J.; Tang, J.-H.; Szidat, S.N. Radiocarbon-based source apportionment of carbonaceous aerosols at a regional background site on Hainan Island, South China. *Environ. Sci. Technol.* **2014**, *48*, 2651–2659. [CrossRef]

27. Li, X.; Wang, S.; Duan, L.; Hao, J.; Li, C.; Chen, Y.; Yang, L. Particulate and Trace Gas Emissions from Open Burning of Wheat Straw and Corn Stover in China. *Environ. Sci. Technol.* **2007**, *41*, 6052–6058. [CrossRef]

28. Ni, H.; Tian, J.; Wang, X.; Wang, Q.; Han, Y.; Cao, J.; Dusek, U. $PM_{2.5}$ emissions and source profiles from open burning of crop residues. *Atmos. Environ.* **2017**, *169*, 229–237. [CrossRef]

29. Turn, S.Q.; Jenkins, B.M.; Chow, J.C.; Pritchett, L.C.; Campbell, D.; Cahill, T.; Whalen, S.A. Elemental characterization of particulate matter emitted from biomass burning: Wind tunnel derived source profiles for herbaceous and wood fuels. *J. Geophys. Res. Atmos.* **1997**, *102*, 3683–3699. [CrossRef]

30. Zhang, H.; Wang, S.; Hao, J.; Wan, L.; Jiang, J.; Zhang, M.; Mellouki, A.W. Chemical and size characterization of particles emitted from the burning of coal and wood in rural households in Guizhou, China. *Atmos. Environ.* **2012**, *51*, 94–99. [CrossRef]

31. Shen, Z.; Cao, J.; Arimoto, R.; Han, Z.; Zhang, R.; Han, Y.; Tanaka, S. Ionic composition of TSP and $PM_{2.5}$ during dust storms and air pollution episodes at Xi'an, China. *Atmos. Environ.* **2009**, *43*, 2911–2918. [CrossRef]

32. Watson, J.G.; Chow, J.C.; Houck, J.E. $PM_{2.5}$ chemical source profiles for vehicle exhaust, vegetative burning, geological material, and coal burning in Northwestern Colorado during 1995. *Chemosphere* **2001**, *43*, 1141–1151. [CrossRef] [PubMed]

33. Hu, Q.; Zhang, L.; Evans, G.J.; Yao, X. Variability of atmospheric ammonia related to potential emission sources in downtown Toronto, Canada. *Atmos. Environ.* **2014**, *99*, 365–373. [CrossRef]

34. Pathak, R.K.; Yao, X.; Chan, C.K. Sampling artifacts of acidity and ionic species in $PM_{2.5}$. *Environ. Sci. Technol.* **2004**, *38*, 254–259. [CrossRef]

35. Rozante, J.R.; Rozante, V.; Souza Alvim, D.; Ocimar Manzi, A.; Barboza Chiquetto, J.; Siqueira D'Amelio, M.T.; Moreira, D.S. Variations of Carbon Monoxide Concentrations in the Megacity of São Paulo from 2000 to 2015 in Different Time Scales. *Atmosphere* **2017**, *8*, 81. [CrossRef]

36. Wofsy, S.C.; McConnell, J.C.; McElroy, M.B. Atmospheric CH_4, CO, and CO_2. *J. Geophys. Res.* **1972**, *77*, 4477–4493. [CrossRef]

37. Zhang, Y.; Lang, J.; Cheng, S.; Li, S.; Zhou, Y.; Chen, D.; Wang, H. Chemical composition and sources of PM1 and $PM_{2.5}$ in Beijing in autumn. *Sci. Total Environ.* **2018**, *630*, 72–82. [CrossRef]

38. Xu, W.; Liu, X.; Liu, L.; Dore, A.J.; Tang, A.; Lu, L.; Zhang, F. Impact of emission controls on air quality in Beijing during APEC 2014: Implications from water-soluble ions and carbonaceous aerosol in $PM_{2.5}$ and their precursors. *Atmos. Environ.* **2019**, *210*, 241–252. [CrossRef]

39. Jaffe, D.; Mahura, A.; Kelley, J.; Atkins, J.; Novelli, P.C.; Merrill, J. Impact of Asian emissions on the remote North Pacific atmosphere: Interpretation of CO data from Shemya, Guam, Midway and Mauna Loa. *J. Geophys. Res. Atmos.* **1997**, *102*, 28627–28635. [CrossRef]

40. Wagstrom, K.M.; Pandis, S.N. Contribution of long range transport to local fine particulate matter concerns. *Atmos. Environ.* **2011**, *45*, 2730–2735. [CrossRef]

41. Huy, D.H.; Thanh, L.T.; Hien, T.T.; Takenaka, N. Development and application of a simultaneous measurement method for gaseous ammonia and particulate ammonium in ambient air. *Aerosol Sci. Technol.* **2016**, *50*, 959–970. [CrossRef]

42. Pathak, R.K.; Wu, W.S.; Wang, T. Summertime $PM_{2.5}$ ionic species in four major cities of China: Nitrate formation in an ammonia-deficient atmosphere. *Atmos. Chem. Phys.* **2009**, *9*, 1711–1722. [CrossRef]

43. Veefkind, J.P.; Aben, I.; McMullan, K.; Förster, H.; de Vries, J.; Otter, G.; Levelt, P.F. TROPOMI on the ESA Sentinel-5 Precursor: A GMES mission for global observations of the atmospheric composition for climate, air quality and ozone layer applications. *Remote Sens. Environ.* **2012**, *120*, 70–83. [CrossRef]

44. Ashbaugh, L.L.; Malm, W.C.; Sadeh, W.Z. A residence time probability analysis of sulfur concentrations at Grand Canyon National Park. *Atmos. Environ.* **1985**, *19*, 1263–1270. [CrossRef]

45. Gao, N.; Cheng, M.-D.; Hopke, P.K. Receptor modeling of airborne ionic species collected in SCAQS. *Atmos. Environ.* **1994**, *28*, 1447–1470. [CrossRef]

46. Hsu, Y.-K.; Holsen, T.M.; Hopke, P.K. Comparison of hybrid receptor models to locate PCB sources in Chicago. *Atmos. Environ.* **2003**, *37*, 545–562. [CrossRef]

47. Lai, S.-o.; Holsen, T.M.; Hopke, P.K.; Liu, P. Wet deposition of mercury at a New York state rural site: Concentrations, fluxes, and source areas. *Atmos. Environ.* **2007**, *41*, 4337–4348. [CrossRef]

48. Chow, J.C.; Watson, J.G.; Crow, D.; Lowenthal, D.H.; Merrifield, T. Comparison of IMPROVE and NIOSH carbon measurements. *J. Aerosol Sci.* **2001**, *34*, 23–34. [CrossRef]

49. Merico, E.; Cesari, D.; Dinoi, A.; Gambaro, A.; Barbaro, E.; Guascito, M.R.; Contini, D. Inter-comparison of carbon content in PM_{10} and $PM_{2.5}$ measured with two thermo-optical protocols on samples collected in a Mediterranean site. *Environ. Sci. Pollut. Res.* **2019**, *26*, 29334–29350. [CrossRef]

50. Hitzenberger, R.; Petzold, A.; Bauer, H.; Ctyroky, P.; Pouresmaeil, P.; Laskus, L.; Puxbaum, H. Intercomparison of thermal and optical measurement methods for elemental carbon and black carbon at an urban location. *Environ. Sci. Technol.* **2006**, *40*, 6377–6383. [CrossRef]

51. Khan, B.; Hays, M.D.; Geron, C.; Jetter, J. Differences in the OC/EC ratios that characterize ambient and source aerosols due to thermal-optical analysis. *Aerosol Sci. Technol.* **2012**, *46*, 127–137. [CrossRef]

52. Ram, K.; Sarin, M.; Tripathi, S. Inter-comparison of thermal and optical methods for determination of atmospheric black carbon and attenuation coefficient from an urban location in northern India. *Atmos. Res.* **2010**, *97*, 335–342. [CrossRef]

53. Cesari, D.; Merico, E.; Dinoi, A.; Marinoni, A.; Bonasoni, P.; Contini, D. Seasonal variability of carbonaceous aerosols in an urban background area in Southern Italy. *Atmos. Res.* **2018**, *200*, 97–108. [CrossRef]

54. Massabò, D.; Caponi, L.; Bove, M.; Prati, P. Brown carbon and thermal–optical analysis: A correction based on optical multi-wavelength apportionment of atmospheric aerosols. *Atmos. Environ.* **2016**, *125*, 119–125. [CrossRef]

55. Cheng, Y.; He, K.-B.; Engling, G.; Weber, R.; Liu, J.-M.; Du, Z.-Y.; Dong, S.-P. Brown and black carbon in Beijing aerosol: Implications for the effects of brown coating on light absorption by black carbon. *Sci. Total Environ.* **2017**, *599*, 1047–1055. [CrossRef]

56. Atkinson, R. Atmospheric chemistry of VOCs and NOx. *Atmos. Environ.* **2000**, *34*, 2063–2101. [CrossRef]

57. Monod, A.; Sive, B.C.; Avino, P.; Chen, T.; Blake, D.R.; Sherwood Rowland, F. Monoaromatic compounds in ambient air of various cities: A focus on correlations between the xylenes and ethylbenzene. *Atmos. Environ.* **2001**, *35*, 135–149. [CrossRef]

58. Fang, X.; Park, S.; Saito, T.; Tunnicliffe, R.; Ganesan, A.L.; Rigby, M.; Prinn, R.G. Rapid increase in ozone-depleting chloroform emissions from China. *Nat. Geosci.* **2019**, *12*, 89–93. [CrossRef]

59. Wallington, T.J.; Bilde, M.; Møgelberg, T.E.; Sehested, J.; Nielsen, O.J. Atmospheric Chemistry of 1,2-Dichloroethane: UV Spectra of $CH_2ClCHCl$ and $CH_2ClCHClO_2$ Radicals, Kinetics of the Reactions of $CH_2ClCHCl$ Radicals with O_2 and $CH_2ClCHClO_2$ Radicals with NO and NO_2, and Fate of the Alkoxy Radical $CH_2ClCHClO$. *J. Phys. Chem.* **1996**, *100*, 5751–5760. [CrossRef]

60. Wu, R.; Wang, S.; Wang, L. Atmospheric oxidation mechanism of chlorobenzene. *Chemosphere* **2014**, *111*, 537–544. [CrossRef]

61. McCulloch, A. Chloroform in the environment: Occurrence, sources, sinks and effects. *Chemosphere* **2003**, *50*, 1291–1308. [CrossRef] [PubMed]

62. Bunce, N.J.; Liu, L.; Zhu, J.; Lane, D.A. Reaction of Naphthalene and Its Derivatives with Hydroxyl Radicals in the Gas Phase. *Environ. Sci. Technol.* **1997**, *31*, 2252–2259. [CrossRef]